

# Transition behavior of PS-*b*-PMMA films on the balanced interfacial interactions

Eunhye Kim<sup>a</sup>, Seunghoon Choi<sup>a</sup>, Rui Guo<sup>a</sup>, Du Yeol Ryu<sup>a,\*</sup>, Craig J. Hawker<sup>b</sup>, Thomas P. Russell<sup>c</sup>

<sup>a</sup> Department of Chemical and Biomolecular Engineering, Yonsei University, Seoul 120-749, Republic of Korea

<sup>b</sup> Material Research Laboratory and Departments of Materials, Chemistry and Biochemistry, University of California, Santa Barbara, CA 93016, United States

<sup>c</sup> Department of Polymer Science & Engineering, University of Massachusetts, Amherst, MA 01003, United States

## ARTICLE INFO

### Article history:

Received 17 August 2010

Received in revised form

23 October 2010

Accepted 29 October 2010

Available online 3 November 2010

### Keywords:

Block copolymers

Thin film

Transition behavior

## ABSTRACT

The thickness dependence of the order-to-disorder transition (ODT), measured by *in situ* grazing-incidence small-angle X-ray scattering (GISAXS), has been investigated in thin films of a symmetric polystyrene-*b*-poly(methyl methacrylate) (PS-*b*-PMMA) on a random copolymer (P(*S-r-MMA*)) grafted to the substrate where the interfacial interactions are balanced. With decreasing film thickness less than  $25L_0$ , the ODT significantly decreases to 193 °C for film of  $10L_0$  in thickness, because the interfacial interactions by a random copolymer grafted to the substrate provide a surface-induced compatibilization toward two block components. However, a plateau of the ODT at  $\sim 213$  °C for films thicker than  $25L_0$  was observed above the bulk value of 200 °C. The elevation of this ODT indicates a suppression of compositional fluctuations normal to the film surface, more than likely because the dominant orientation of the lamellar microdomains was found to be parallel to the film surface.

© 2010 Elsevier Ltd. All rights reserved.

## 1. Introduction

Block copolymer (BCP) self-assembly in thin films has recently been the focus of increased research interest due to their potential use as templates and scaffolds for the fabrication of nanostructured materials [1–5]. These potential applications have stimulated numerous studies on the influence of controlled interfacial interactions, confinement structure, and morphology of BCPs in thin films [6–23]. The Flory–Huggins interaction parameter ( $\chi$ ) between the two block components is inversely proportional to temperature ( $\chi$  decreases with increasing temperature) and the order-to-disorder transition (ODT) is governed by the product of  $\chi \cdot N$ , where  $N$  is the overall number of segments [24,25]. Hence, a phase-mixed or disordered state can be observed when  $\chi \cdot N < 10.495$  in the weak segregation regime. In addition, the phase behavior in a thin film geometry that confines polymer chains to the interfaces will be influenced by the interfacial interactions at substrate/polymer and polymer/air and the commensurability between the equilibrium period ( $L_0$ ) of the BCP and the total film thickness [26–28].

Generally, the microdomains in BCP films of  $\sim L_0$  orient normal to the film surface when the interfacial interactions are balanced (or neutral toward the two block components) and film thickness is

commensurate with  $L_0$  [10–14,29–35]. In contrast, the preferential interactions of one block component with an interface and/or the difference of surface tension between two block components will lead to an orientation of the BCP microdomains parallel to the film surface [6–8,17,36,37]. In developing neutral surfaces, random copolymer (A-*r*-B) approaches to balancing interfacial interactions have been successfully developed for surface modification using either a chemical grafting or cross-linking strategy, enabling the microdomains of block copolymer (A-*b*-B) to orient normal to the film surface [10–13,15,19,33–35,38]. Simulation studies on BCPs confined between two neutral walls indicate that the ODT in consideration of the fluctuation effect is strongly suppressed for  $L_0 < 1$ , but consistently increased up to 10% with respect to the mean-field value of  $\chi N = 10.495$ , which is in agreement with the analytical studies of confinement effects on the ODT in the BCP melts [39,40].

Recently, the ODT and order-to-order transition (OOT) in thin films of BCPs were investigated by *in situ* grazing-incidence small-angle X-ray scattering (GISAXS) [41–44]. For films of a lamella-forming polystyrene-*b*-polyisoprene (PS-*b*-PI) on PS grafted substrates, the thickness dependence of the ODT showed a plateau in the value of the ODT for films over  $12L_0$ , which is still higher than that observed in the bulk PS-*b*-PI. The ODT was found to increase rapidly with decreasing film thickness. In contrast, the plateau value of the ODT for films on bare Si wafers was nearly identical to that found in the bulk, due to the weak interactions between the BCP and substrate at the oxide/polymer interface [41]. For films of

\* Corresponding author. Tel.: +82 2 2123 5756; fax: +82 2 312 6401.  
E-mail address: [dyryu@yonsei.ac.kr](mailto:dyryu@yonsei.ac.kr) (D.Y. Ryu).

polystyrene-*b*-poly(methyl methacrylate) (PS-*b*-PMMA) on PS grafted substrates, a gradual increase in ODT rather than a plateau value of the ODT, was observed with decreasing film thickness, which can be correlated to the weak temperature dependence of  $\chi$  between PS and PMMA in comparison to that of PS and PI [42]. Moreover, the PS grafted substrates that favor the PS component of BCP promote an orientation of the lamellar microdomains parallel to the substrate interface, which may in turn be related to the suppression of the compositional fluctuations in BCP films.

In this study, we present the ODT behavior in thin films of PS-*b*-PMMA on surfaces to which a random copolymer (P(S-*r*-MMA)) has been grafted where the interfacial interactions are balanced. The thickness dependence of ODT was probed by *in situ* GISAXS measurements. With decreasing film thickness less than  $25L_0$ , a rapid decrease in the ODT for the films on a neutral surface can be attributed to a surface-induced compatibilization toward two block components. This result is in contrast to an increase in the ODT for the BCP films on surfaces having an affinity for one block component. However, similar to these films, the ODT for films thicker than  $25L_0$  exhibiting a majority orientation of the lamellar microdomains parallel to the film surface reached a plateau value above that for the bulk.

## 2. Experimental

A nearly symmetric PS-*b*-PMMA was purchased from Polymer Source with the number-average molecular weight ( $M_n$ ) and polydispersity index ( $M_w/M_n$ ), characterized by size-exclusion chromatography (SEC), of 29,000 g/mol and 1.08, respectively. The volume fraction of PS ( $\Phi_{ps}$ ) in the BCP was determined to be 0.553 by  $^1\text{H}$  nuclear magnetic resonance ( $^1\text{H}$  NMR) based on the mass densities of two components (1.05 and 1.184 g/cm<sup>3</sup> for PS and PMMA). A hydroxyl end-functionalized random copolymer composed of styrene (S) and methyl methacrylate (MMA), denoted as P(S-*r*-MMA), was synthesized by a nitroxide-mediated living free radical polymerization [10]. The  $M_n$  and  $M_w/M_n$  of P(S-*r*-MMA) are approximately 10,000 g/mol and <1.30, respectively, where the volume fraction of S was 0.59 (mole fraction of 0.55) to balance the interfacial interactions with the substrate toward the PS and PMMA block components of the lamellar forming BCP [13,19].

P(S-*r*-MMA) grafting to the substrate was done by thermally annealing thin films of hydroxyl-terminated P(S-*r*-MMA) on cleaned Si wafer under vacuum at 170 °C for 3 days, well above the glass transition temperatures ( $T_g$ ) of both PS (100 °C) and PMMA (115 °C). During this process, end-functional hydroxyl groups of the random copolymer can diffuse to the substrate and react with the native oxide layer, resulting in polymer chains grafted on the substrate. The thickness of the grafted P(S-*r*-MMA) was found to be  $\sim 5 \pm 0.3$  nm by ellipsometry (SE MG-1000, Nano-view Co.) at an incidence angle of 70° after rinsing with toluene to remove unattached polymer chains. BCP films of thicknesses ranging from 196 ( $10L_0$ ) to 980 nm ( $50L_0$ ) were spin-coated from toluene solution onto the random copolymer grafted substrate.  $L_0 = 19.6$  nm is consistent with the inter-lamellar spacing by  $d = 2\pi/q^*$ , where the asterisk indicates a primary maximum peak position of the scattering vector ( $q$ ). The films were annealed at 170 °C under vacuum for 3 days to allow for sufficient chain mobility between  $T_g$  and the ODT.

Grazing-incidence small-angle X-ray scattering (GISAXS) experiments were carried out at the 4C2 beam-line of the Pohang Accelerator Laboratory (PAL), Pohang, Korea [45]. The operating conditions were set to a wavelength of 1.38 Å and the sample-to-detector distance of 2.2 m. The film samples were mounted in a heating cell under vacuum and incidence angle was in the range of 0.165°–0.175°, well above the critical angle (0.156°) of PS-*b*-PMMA films [46]. 2D GISAXS patterns were recorded using a CCD

detector positioned at the end of a vacuum guide tube when the X-ray beam passes through BCP thin films. Small-angle X-ray scattering (SAXS; 4C1 beam-line) was used to obtain the microdomain morphologies of the block copolymers in the bulk. To minimize sample degradation by the X-ray beam, a minimal exposure time of 10–60 s was used [42]. All the heating experiments were automatically controlled with a PID temperature controller from 140 to 235 °C at a constant heating rate of 0.9 °C/min.

The cross-sectional structure of PS-*b*-PMMA films was investigated by transmission electron microscopy (TEM; S-7600, Hitachi) operated at 100 kV. A thin carbon layer was first evaporated at air/polymer interface, followed by embedding with epoxy resin kit (Araldite 502, Polysciences). After curing the epoxy resin at 60 °C for 12 h, the epoxy-embedding film was peeled off from the substrate in liquid nitrogen. The polymer/substrate interface was again treated with thin carbon layer and epoxy resin kit in a similar manner. Thin sections ( $\sim 50$  nm) from the epoxy-embedding film were obtained using an ultramicrotome (Leica EM UC6) with a diamond knife. To enhance the electron density contrast between two phases, the PS block component was selectively stained with RuO<sub>4</sub>.

## 3. Results and discussion

Grazing-incidence small-angle X-ray scattering (GISAXS) was used to determine the internal structure of the BCP films by probing both the near surface and the entire film structure at an incidence angle ( $\alpha_i$ ). This technique has recently provided the detailed analysis of the characteristic patterns for nanostructures due to overall tracking of a large scattering volume [45,46]. Fig. 1a shows the GISAXS patterns for a PS-*b*-PMMA film of  $40L_0$  (784 nm) on a random copolymer (P(S-*r*-MMA)) grafted substrate, which was measured at room temperature after thermally annealing the film at 170 °C for 3 days under vacuum. In the grazing-incidence scattering geometry used,  $q_{xy}$  is the scattering vector normal to the incidence plane, which is related to  $d$ -spacing of the film by  $d = 2\pi/q_{xy}^*$  at the primary peak position, and  $q_z$  is the scattering vector normal to the sample surface, defined as  $q_z = (4\pi/\lambda) \sin \theta$ . Incidence angle ( $\alpha_i$ ) was varied from 0.110 to 0.165°, i.e. through the critical angle ( $\alpha_c = 0.156^\circ$ ) of PS-*b*-PMMA in order to probe the depth dependence of the morphology in the film [46,47].

GISAXS patterns measured at  $\alpha_i = 0.125^\circ$ , below the critical angle of the BCP film, provides information on the near surface structure (to  $\sim 6$  nm) of film less than  $L_0$ . As incidence angle is increased up to 0.145°, the intensities for the *hidden* scattering peaks along  $q_z$  near  $q_{xy} = 0$  (behind the beam stop) and the *in-plane* scattering peaks along  $q_{xy}$  at  $q_z = 0$  are enhanced due to the increased scattering volume underneath the film surface (to  $\sim 11$  nm). GISAXS experiments were also performed at incidence angles between the critical angles of the BCP and the silicon substrate so as to obtain structural information for the entire films. For  $\alpha_i = 0.165^\circ$ , two intense *hidden* scattering peaks (marked with A zone) along  $q_z$  near  $q_{xy} = 0$  can be attributed to the orientation of the lamellar microdomains parallel to the film surface [48,49], as presented by the TEM image in Fig. 2. The parallel microdomain orientation to the film surface where the interfacial interactions are balanced might not be surprising for the following reasons. Under neutral conditions, either of block components can be located at the substrate (or surface interface) with no energetic penalty. If there are, however, a sufficient number of lamellae in the film, any frustration effects arising from incommensurability between film thickness and the period of the BCP would only require a minimal perturbation to the BCP (compression or extension of the BCP chains). These could easily be offset by even a slight difference in surface energies that favors either of block components. Accordingly, this orientation of the lamellar microdomains parallel to the

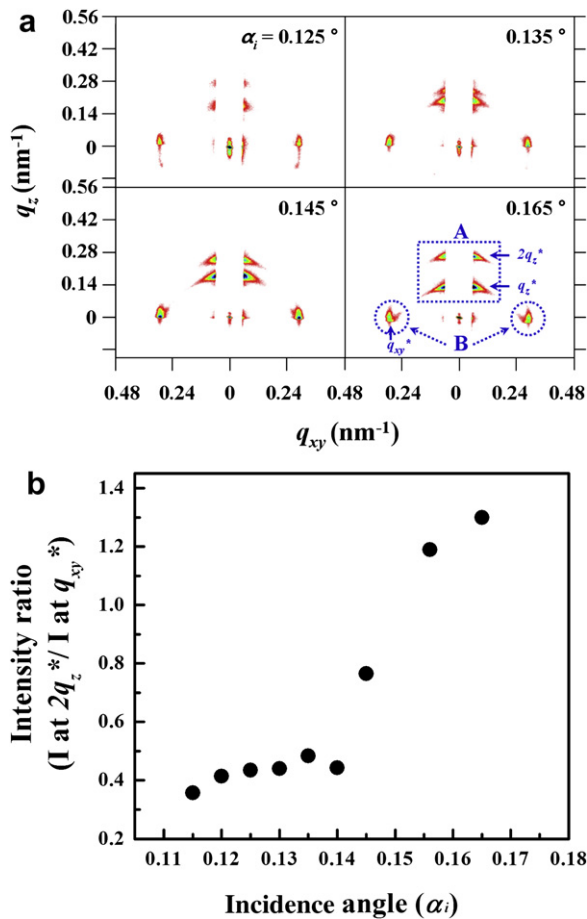


**Fig. 1.** (a) GISAXS patterns for a PS-*b*-PMMA film of  $40L_0$  (784 nm) on a random copolymer (P(S-*r*-MMA)) grafted substrate, which was measured at room temperature after thermally annealing the film at 170 °C for 3 days under vacuum. Incidence angle was varied from 0.110° to 0.165°, where the critical angle ( $\alpha_c$ ) of PS-*b*-PMMA films is 0.156°. Two intense *hidden* scattering peaks and symmetric *in-plane* scattering peaks are marked with A and B zones. (b) Intensity ratio of the *hidden* scattering peak (at  $2q_z^*$ ) to the *in-plane* scattering peak (at  $q_{xy}^*$ ) as a function of incidence angle.

film surface, as a promising consequence of frustration, can be distributed over all the lamellae.

On the other hand, two *in-plane* scattering peaks (marked with B zone at  $\alpha_i = 0.165^\circ$ ) along  $q_{xy}$  at  $q_z = 0$  may be attributed to the presence of lamellar microdomain aligned nonparallel but close to

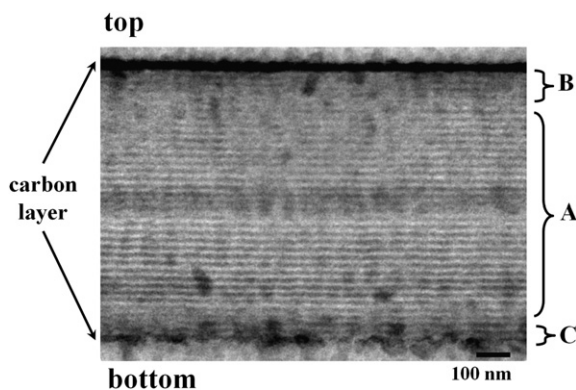


**Fig. 2.** The cross-sectional TEM image for PS-*b*-PMMA film of  $40L_0$  (784 nm) on a random copolymer (P(S-*r*-MMA)) grafted substrate. Three feature zones involve a majority sub-surface layer (A zone) of lamellae aligned parallel to the film surface, the surface layer (B zone), and the substrate interface where the interfacial interactions are balanced (C zone)  $\sim 1L_0$ .

normal to the film surface presumably at both air/polymer and polymer/substrate interfaces, because an increased intensity with increasing incidence angle up to  $\alpha_i = 0.145^\circ$  indicates the near surface structure (depth to  $\sim 11$  nm) of film and the perpendicular microdomain orientation is expected the near substrate ( $\sim L_0$ ) where the interfacial interactions are balanced. In addition to the latter, this is also to be expected due to the similar surface tensions for two block components at no cost energetically, which allow no strong preference for either of block components at the air surface. Of particular note are the minimal ring patterns from the reflected and transmitted X-ray beams with respect to the film at azimuthal angles other than 0° or 90°. It demonstrates that only two discernible orientations, parallel in major and perpendicular in minor to the film at both air/polymer and polymer/substrate interfaces, are observed at the entire film since any other orientation would require a stretching or compression of the BCP chains and may result in an energetic penalty.

The intensity ratio of the *hidden* scattering peak (at  $2q_z^*$ ) to the *in-plane* scattering peak (at  $q_{xy}^*$ ) is shown in Fig. 1b as a function of incidence angle. In this case, the second maximum of the *hidden* scattering peaks was used since the diffraction peaks by the reflected beam are usually less distorted due to the refraction effect, although a similar result was observed for the intensity ratio of the first maximum of the *hidden* scattering peaks at  $q_z^*$  to the *in-plane* scattering peak. As can be seen, below the critical angle ( $\alpha_c = 0.156^\circ$ ), i.e. probing only the near surface structure of the BCP film, the ratio takes on a value that represents a certain number of lamellae oriented parallel and perpendicular to the film surface. However, as incidence angle is increased, this ratio stays relatively constant up to the critical angle. Above the critical angle, the X-rays penetrate into the entire film and the ratio is seen to increase rapidly. Consequently, the number of lamellae aligned parallel to the film surface at the entire film is much larger, on average, than that at the near surface structure of the BCP film. As discussed above, any perturbations from a balanced interfacial interaction condition or stronger perturbation to the conformation of the BCP chains (i.e. surface roughness) will favor a microdomain orientation parallel to the film surface, as long as commensurability effects are minimal. Fig. 2 shows the cross-sectional TEM image for PS-*b*-PMMA film of  $40L_0$  (784 nm) on a random copolymer (P(S-*r*-MMA)) grafted substrate. A majority sub-surface layer (A zone) distinctly indicates the lamellae aligned parallel to the film surface, while the surface layer (B zone) and substrate interface (C zone of  $\sim 1L_0$ ) where the interfacial interactions are balanced are indiscernible due to the lamellar distortion, which is presumably caused by the presence of lamellar microdomain aligned nonparallel but in part close to normal to the film surface.

Fig. 3 shows a series of *in situ* 2D GISAXS patterns for PS-*b*-PMMA film of  $50L_0$  (980 nm) on a random copolymer (P(S-*r*-MMA)) grafted substrate, at which the patterns were measured at each temperature during heating from 140 to 235 °C at a rate of 0.9 °C/min after thermally annealing the film at 170 °C for 3 days under vacuum. Here, incidence angle was fixed at 0.175° above the critical angle for PS-*b*-PMMA films to probe morphology across the entire film thickness. At  $T = 160^\circ\text{C}$ , two intense *hidden* scattering peaks are seen along with *in-plane* scattering peaks, which is consistent with the results for film of  $40L_0$  measured at room temperature (Fig. 1a). Therefore, these characteristic patterns in the film geometry correspond to a majority orientation of the lamellar microdomains parallel to the film surface and a minority of lamellae aligned normal to the surface at both air/polymer and polymer/substrate interface layer. Similar GISAXS patterns are observed up to  $\sim 210^\circ\text{C}$ , which is higher than the ODT (200 °C) of the bulk PS-*b*-PMMA. With further increasing temperature to  $T > 212^\circ\text{C}$ , the *in-plane* scattering peaks (along  $q_{xy}$ ) broaden and

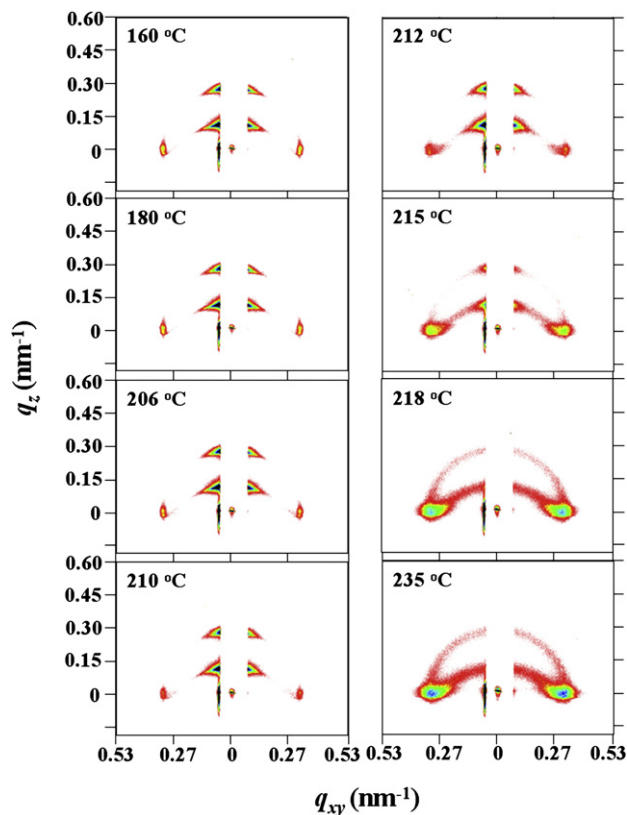


**Fig. 3.** A series of *in situ* 2D GISAXS patterns for PS-*b*-PMMA film of 50L<sub>0</sub> (980 nm) on a random copolymer (P(S-*r*-MMA)) grafted substrate, which was measured at each temperature during heating 130–235 °C at a rate of 0.9 °C/min after thermally annealing the film at 170 °C for 3 days under vacuum. Here, incidence angle was fixed at 0.175° above the critical angle for PS-*b*-PMMA films.

the *hidden* scattering peaks (along  $q_z$ ) diminish significantly. At  $T = 235$  °C, the scattering consists of two diffuse elliptical scattering patterns since a superposition of the correlation hole scatterings arising from a disordered (phase-mixed) state contribute to the scattered intensity [42].

To determine the transition temperature in the BCP films, the intensity profiles from the GISAXS patterns in Fig. 3 were scanned along the  $q_z$ -direction near  $q_{xy} = 0$  (behind the beam stop) and along the  $q_{xy}$ -direction at constant  $q_z = 0$  as a function of temperature, as shown in Fig. 4a and b, respectively. The first and second maxima of the *hidden* scattering intensity in Fig. 4a, caused by the scattering by the transmitted and reflected beam to the films, respectively, arise from the lamellar microdomains parallel to the film surface. Over the temperature range to 235 °C, the *hidden* scattering peaks in the ordered state for  $T < 212$  °C in Fig. 4a are much sharper than the *in-plane* scattering peaks in the disordered state for  $T > 212$  °C in Fig. 4b. The temperature dependence of both the peak intensities and full-width at half-maximum (FWHM) of *in-plane* scattering peaks enable us to determine the ODT in the BCP film, as plotted in Fig. 4c. A sudden decrease in intensity of the second maximum (at  $2q_z^*$ ) for the *hidden* scattering peaks and a noticeable decrease in intensity of *in-plane* scattering (at  $q_{xy}^*$ ) with discontinuous change of FWHM reflect the structural change of the entire film during heating, leading to an ODT of  $213 \pm 3$  °C for PS-*b*-PMMA film of 50L<sub>0</sub>. Transition temperature was also measured to be analogous to that for films of 40L<sub>0</sub> and 25L<sub>0</sub> on a random copolymer (P(S-*r*-MMA)) grafted substrate, and these were still above the ODT (200 °C) of the bulk PS-*b*-PMMA. It should be noted that for the *in-plane* scattering at  $q_{xy}^*$  the high intensity below the

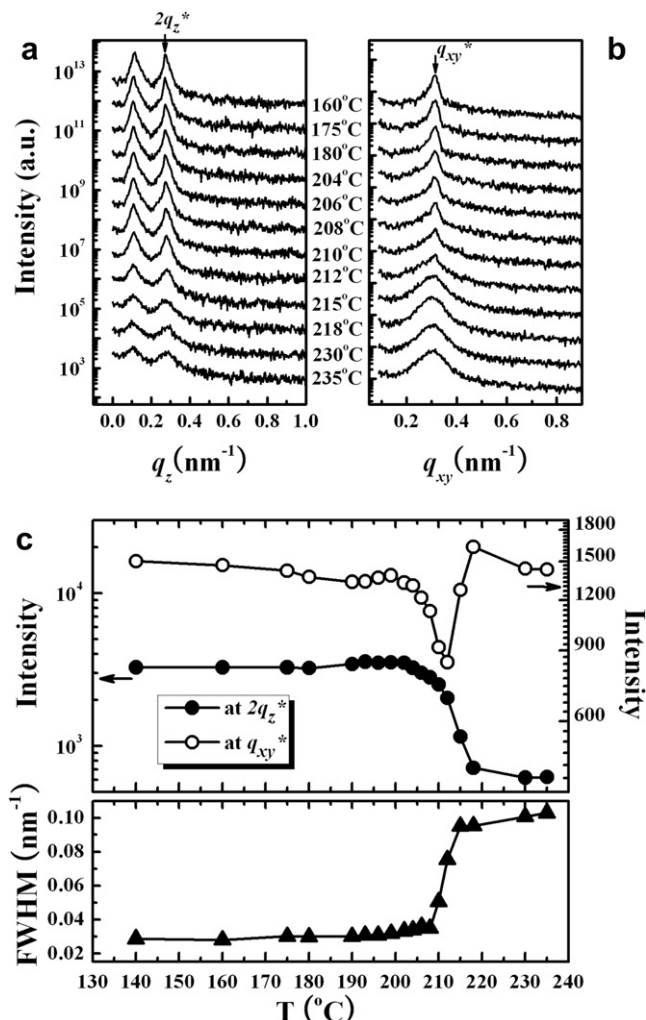


**Fig. 4.** Intensity profiles from the GISAXS patterns in Fig. 3 for PS-*b*-PMMA film of 50 (980 nm) on a random copolymer (P(S-*r*-MMA)) grafted substrate as a function of temperature. (a) The *hidden* scattering intensity scanned along  $q_z$ -direction near  $q_{xy} = 0$  (behind the beam stop) and (b) the *in-plane* scattering scanned along  $q_{xy}$ -direction at constant  $q_z = 0$ . The profiles were shifted by the factor of 6–7. (c) Peak intensities as a function of temperature for both the *hidden* scattering at  $2q_z^*$  and the *in-plane* scattering at  $q_{xy}^*$ , and full-width at half-maximum (FWHM) of *in-plane* scattering peaks. An ODT of  $213 \pm 3$  °C was determined for this film.

ODT can be attributed to a surface layer composed of a minority of lamellae aligned normal to the surface.

The positions of the primary maximum peak ( $q^*$ ) are shown in Fig. 5 as a function of temperature for bulk PS-*b*-PMMA and a thick film of 50L<sub>0</sub>, where  $q_{xy}^*$  and  $2q_z^*$  indicate the peak positions of the first maximum in the *in-plane* scattering and the second maximum in the *hidden* scattering, respectively. With increasing temperature, a slight increase in  $q^*$  is seen for bulk PS-*b*-PMMA up to the ODT (200 °C) and a rapid increase over the ODT, indicating that  $d$ -spacing decreases in the disordered state since the Flory–Huggins segmental interaction parameter ( $\chi$ ) between the two block components is inversely proportional to temperature. For a PS-*b*-PMMA film of 50L<sub>0</sub>, the discontinuous changes in  $q_{xy}^*$  and  $2q_z^*$  reflect the ODT for the film, which parallel the temperature dependences of the peak intensities shown in Fig. 4c. Above the ODT,  $q_{xy}^*$  corresponding to the *in-plane*  $d$ -spacing remains relatively constant, while  $2q_z^*$  corresponding to the *out-of-plane*  $d$ -spacing (perpendicular to the film surface) increases slightly. Keeping in mind that the volume of the BCP films must remain constant due to the incompressibility of polymers, and taking into account the thermal expansion coefficient, a significant

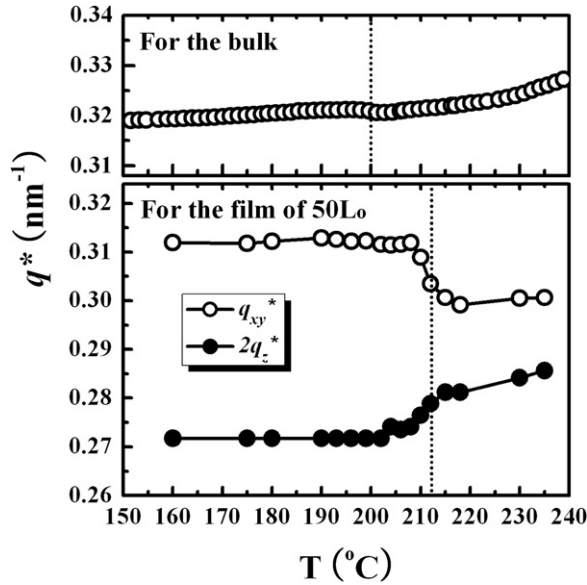
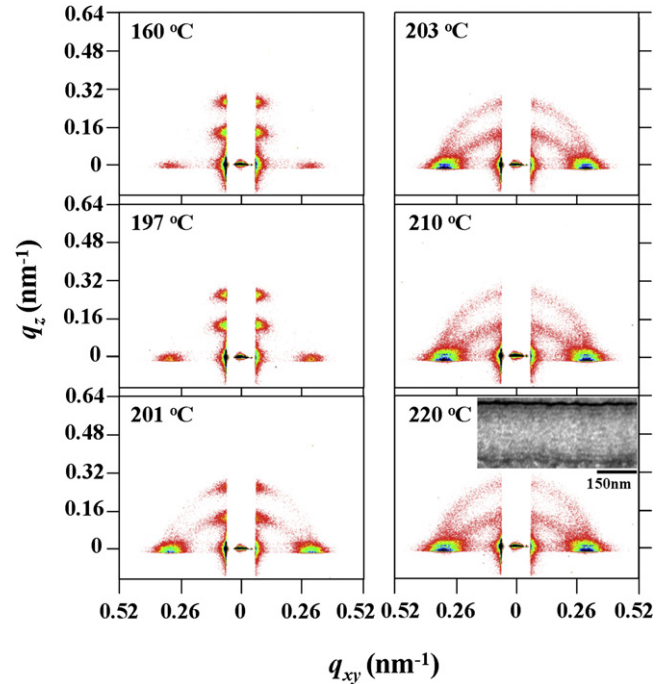


**Fig. 5.** Positions of the primary maximum peak ( $q^*$ ) as a function of temperature for (a) the bulk PS-*b*-PMMA and (b) the film of  $50L_0$ .  $q_{xy}^*$  and  $2q_z^*$  are the peak positions of the first maximum in the *in-plane* scattering and the second maximum in the *hidden* scattering, respectively.

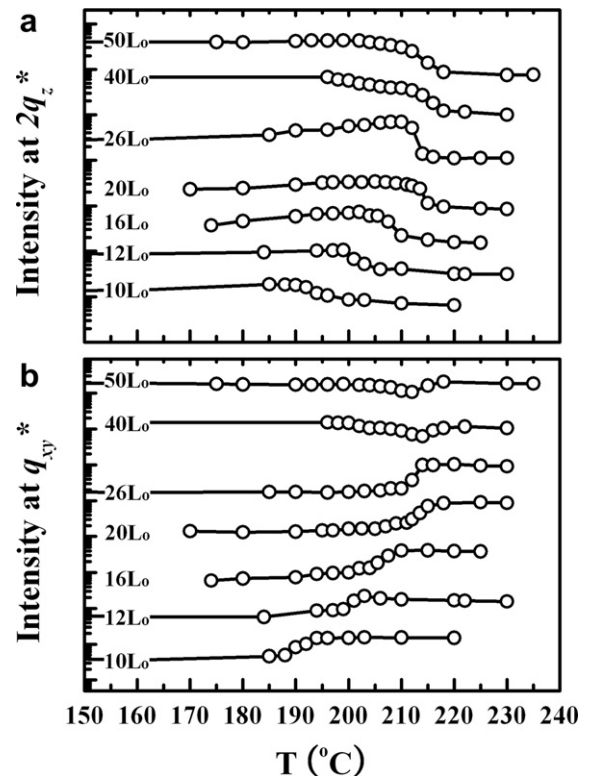
decrease of  $q_{xy}^*$  and a complementary increase of  $2q_z^*$  at the ODT demonstrate that a major relaxation (or a decrease of the *out-of-plane* *d*-spacing) of the block chains in the majority lamellar microdomains oriented parallel to the film surface compensates for an increase of the *in-plane* *d*-spacing due to the random chain conformation in the disordered film. This feature in the film geometry can be a consequence of a majority orientation of the lamellar microdomains parallel to the film surface due to the greater degree of stretching for block copolymer chains along the normal direction to the film surface.

Fig. 6 shows a series of *in situ* 2D GISAXS patterns at a fixed exposure time of 20 s for the PS-*b*-PMMA film of  $12L_0$  (235 nm) at an incidence angle at  $0.160^\circ$  on P(S-*r*-MMA) grafted substrate. At  $T = 160^\circ\text{C}$  for film of  $12L_0$ , two *hidden* scattering peaks can be correlated to the lamellar microdomains aligned parallel to the film surface. These are analogous to those for films of  $40L_0$ ,  $25L_0$ , and the others, although the peak intensities in the *in-plane* scattering along  $q_{xy}$  are weaker due to the thickness effect. With further increasing temperature to  $220^\circ\text{C}$ , the *in-plane* scattering peaks (along  $q_{xy}$ ) broaden significantly with two diffuse elliptical scattering patterns at the cost of the *hidden* scattering peaks (along  $q_z$ ). The intensity changes in the *hidden* and *in-plane* scattering peaks lead to an ODT  $\sim 202^\circ\text{C}$ , which is much lower than the ODT ( $213^\circ\text{C}$ ) for film of  $50L_0$ . The GISAXS pattern for the disordered BCP film at  $T = 220^\circ\text{C}$  corresponds well to the TEM image of samples in the inset, indicating the compositional fluctuations in the BCP films.

The peak intensities for the *hidden* scattering (at  $2q_z^*$ ) and the *in-plane* scattering (at  $q_{xy}^*$ ) are plotted in Fig. 7 as a function of temperature and film thickness. It was found that the discontinuous change in the intensity of the *hidden* scattering (at  $2q_z^*$ ) coincides with a noticeable decrease (or discontinuous change) in the *in-plane* scattering, as described in Fig. 4. This behavior also reflects the structural change of the entire BCP films undergoing a transition from the ordered to disordered state, leading to a thickness dependent ODT behavior for the PS-*b*-PMMA films. When film thickness is  $10L_0$ , the ODT is observed to significantly decrease to  $193^\circ\text{C}$ . For the *in-plane* scattering, the intensity below the ODT is somewhat higher for films of  $40L_0$  and  $50L_0$  due to a surface layer composed of a plausible minority of lamellae aligned



**Fig. 6.** A series of *in situ* 2D GISAXS patterns for PS-*b*-PMMA film of  $12L_0$  (235 nm) on a random copolymer (P(S-*r*-MMA)) grafted substrate, which was measured at each temperature during heating  $130$ – $235^\circ\text{C}$  at a rate of  $0.9^\circ\text{C}/\text{min}$  after thermally annealing the film at  $170^\circ\text{C}$  for 3 days under vacuum. Here, a constant incidence angle of  $0.160^\circ$  was used. Insets are the corresponding cross-sectional TEM images for films, which were taken after quenching at  $220^\circ\text{C}$  during heating.



**Fig. 7.** Peak intensities for (a) the *hidden* scattering and (b) the *in-plane* scattering as a function of temperature and film thickness. The first maximum (at  $q_{xy}^*$ ) for the *in-plane* scattering and the second maximum (at  $2q_z^*$ ) for the *hidden* scattering were used.

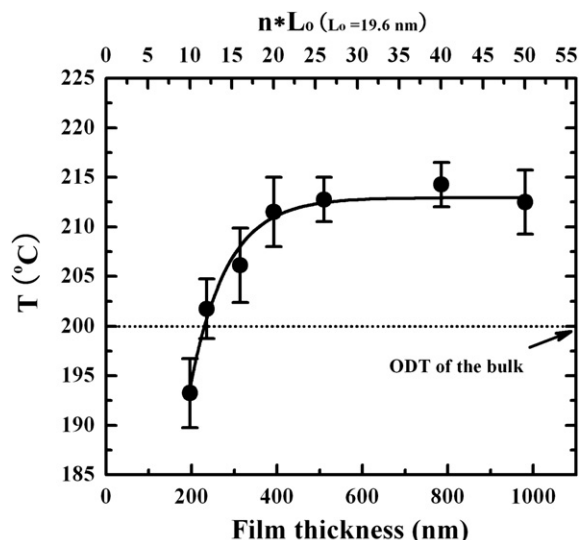


Fig. 8. ODT for PS-*b*-PMMA films on a random copolymer (P(S-*r*-MMA)) grafted substrate as a function of film thickness. A dotted line indicates the ODT (200 °C) of the bulk PS-*b*-PMMA.

normal to the air surface, while it decreases for the other films due to the dominant orientation of the lamellar microdomains parallel to the film surface.

#### 4. Summary

The thickness dependence of ODT for PS-*b*-PMMA films on surface having a grafted random copolymer (P(S-*r*-MMA)) is summarized in Fig. 8. Above all, decreasing film thickness to  $10L_0$  leads to a decrease in the ODT to 193 °C, indicating that in PS-*b*-PMMA films less than  $25L_0$  the interfacial interactions by a random copolymer (P(S-*r*-MMA)) grafted substrate provide a surface-induced compatibilization toward two block components. It was found that the thinner the films, the more effectively the surface field propagates into the film by making them more compatible at the substrate surface. For films of  $25L_0$ ,  $40L_0$ , and  $50L_0$ , the ODT is consistently observed at an elevated temperature of  $\sim 213$  °C, well above the ODT (200 °C) for bulk PS-*b*-PMMA (indicated by a dotted line). A similar plateau in the ODT for films on a PS grafted substrate was observed, where the grafting PS chains preferentially interact with the PS block of PS-*b*-PMMA [42]. Therefore, for the films having a thickness greater than  $25L_0$ , the elevation of the ODT also indicates a suppression of compositional fluctuations normal to the film surface, more than likely because the dominant orientation of the lamellar microdomains was found to be parallel to the film surface. In the case of a sufficient number of lamellae in the film, this orientation in the film geometry may be regarded as any frustration effects arising from incommensurability between film thickness and the period of the BCP. This result illustrates the importance of the interfacial interactions in the transition behavior of the BCP films for further experimental and theoretical consideration.

#### Acknowledgment

This work was supported by the Nuclear R&D Programs, APCPI ERC program (R11-2007-050-00000), and NRF grant (2010-0015410) funded by the Ministry of Education, Science & Technology (MEST), Samsung Electronics fund, Korea, Department of Energy (DOE), Office of Basic Energy Science, and the National Science Foundation (MRSEC Program DMR-0520415), US.

#### References

- [1] Hamley IW. The physics of block copolymers. New York: Oxford University Press; 1998.
- [2] Park C, Yoon J, Thomas EL. *Polymer* 2003;44(22):6725–60.
- [3] Hamley IW. *Progress in Polymer Science* 2009;34(11):1161–210.
- [4] Bang J, Jeong U, Ryu DY, Russell TP, Hawker CJ. *Advanced Materials* 2009;21(47):4769–92.
- [5] Gowd EB, Nandan B, Bigall NC, Eychmüller A, Formanek P, Stamm M. *Polymer* 2010;51(12):2661–7.
- [6] Henkee CS, Thomas EL, Fetters LJ. *Journal of Materials Science* 1988;23(5):1685–94.
- [7] Anastasiadis SH, Russell TP, Satija SK, Majkrzak CF. *Physical Review Letters* 1989;62(16):1852.
- [8] Hasegawa H, Hashimoto T. *Macromolecules* 1985;18(3):589–90.
- [9] Mansky P, Russell TP, Hawker CJ, Mays J, Cook DC, Satija SK. *Physical Review Letters* 1997;79(2):237.
- [10] Mansky P, Liu Y, Huang E, Russell TP, Hawker C. *Science* 1997;275(5305):1458–60.
- [11] Huang E, Russell TP, Harrison C, Chaikin PM, Register RA, Hawker CJ, et al. *Macromolecules* 1998;31(22):7641–50.
- [12] Ryu DY, Shin K, Drockenmüller E, Hawker CJ, Russell TP. *Science* 2005;308(5719):236–9.
- [13] Ham S, Shin C, Kim E, Ryu DY, Jeong U, Russell TP, et al. *Macromolecules* 2008;41(17):6431–7.
- [14] Xu T, Hawker CJ, Russell TP. *Macromolecules* 2005;38(7):2802–5.
- [15] Maire HC, Ibrahim S, Li Y, Ito T. *Polymer* 2009;50(10):2273–80.
- [16] Müller-Buschbaum P, Maurer E, Bauer E, Cubitt R. *Langmuir* 2006;22(22):9295–303.
- [17] Buck E, Fuhrmann J. *Macromolecules* 2001;34(7):2172–8.
- [18] Müller-Buschbaum P, Schulz L, Metwalli E, Moulin JF, Cubitt R. *Langmuir* 2008;24(15):7639–44.
- [19] Ryu DY, Ham S, Kim E, Jeong U, Hawker CJ, Russell TP. *Macromolecules* 2009;42(13):4902–6.
- [20] Lambooy P, Russell TP, Kellogg GJ, Mayes AM, Gallagher PD, Satija SK. *Physical Review Letters* 1994;72(18):2899.
- [21] Walton DG, Kellogg GJ, Mayes AM, Lambooy P, Russell TP. *Macromolecules* 1994;27(21):6225–8.
- [22] Kellogg GJ, Walton DG, Mayes AM, Lambooy P, Russell TP, Gallagher PD, et al. *Physical Review Letters* 1996;76(14):2503.
- [23] Sohn BH, Yun SH. *Polymer* 2002;43(8):2507–12.
- [24] Leibler L. *Macromolecules* 1980;13(6):1602–17.
- [25] Bates FS, Fredrickson GH. *Annual Review of Physical Chemistry* 1990;41(1):525–57.
- [26] Pickett GT, Witten TA, Nagel SR. *Macromolecules* 1993;26(12):3194–9.
- [27] Sommer J-U, Hoffmann A, Blumen A. *The Journal of Chemical Physics* 1999;111(8):3728–32.
- [28] Potemkin II. *Macromolecules* 2004;37(9):3505–9.
- [29] Matsen MW. *The Journal of Chemical Physics* 1997;106(18):7781–91.
- [30] Geisinger T, Muller M, Binder K. *The Journal of Chemical Physics* 1999;111(11):5241–50.
- [31] Tang WH. *Macromolecules* 2000;33(4):1370–84.
- [32] Meng D, Wang Q. *The Journal of Chemical Physics* 2007;126(23):234902–10.
- [33] In I, La Y-H, Park S-M, Nealey PF, Gopalan P. *Langmuir* 2006;22(18):7855–60.
- [34] Ryu DY, Wang J-Y, Lavery KA, Drockenmüller E, Satija SK, Hawker CJ, et al. *Macromolecules* 2007;40(12):4296–300.
- [35] Han E, In I, Park SM, La YH, Wang Y, Nealey PF, et al. *Advanced Materials* 2007;19(24):4448–52.
- [36] Coulon G, Russell TP, Deline VR, Green PF. *Macromolecules* 1989;22(6):2581–9.
- [37] Russell TP, Coulon G, Deline VR, Miller DC. *Macromolecules* 1989;22(12):4600–6.
- [38] Han E, Stuen KO, Leolukman M, Liu C-C, Nealey PF, Gopalan P. *Macromolecules* 2009;42(13):4896–901.
- [39] Bing M, Dadong Y, Charles CH, An-Chang S. *The Journal of Chemical Physics* 2006;124(14):144902.
- [40] Alexander-Katz A, Fredrickson GH. *Macromolecules* 2007;40(11):4075–87.
- [41] Shin C, Ahn H, Kim E, Ryu DY, Huh J, Kim K-W, et al. *Macromolecules* 2008;41(23):9140–5.
- [42] Kim E, Ahn H, Ryu DY, Kim J, Cho J. *Macromolecules* 2009;42(21):8385–91.
- [43] Shin C, Ryu DY, Huh J, Kim JH, Kim K-W. *Macromolecules* 2009;42(6):2157–60.
- [44] Ahn H, Shin C, Lee B, Ryu DY. *Macromolecules* 2010;43(4):1958–63.
- [45] Yoon J, Kim KW, Kim J, Heo K, Jin KS, Jin S, et al. *Macromolecular Research* 2008;124(7):575–85.
- [46] Yoon J, Yang SY, Lee B, Joo W, Heo K, Kim JK, et al. *Journal of Applied Crystallography* 2007;40:305–12.
- [47] Factor BJ, Russell TP, Toney MF. *Physical Review Letters* 1991;66(9):1181.
- [48] Busch P, Rauscher M, Smilgies DM, Posselt D, Papadakis CM. *Journal of Applied Crystallography* 2006;39(3):433–42.
- [49] Busch P, Posselt D, Smilgies DM, Rauscher M, Papadakis CM. *Macromolecules* 2007;40(3):630–40.